Nanoscale

Accepted Manuscript

This article can be cited before page numbers have been issued, to do this please use: Y. S. Khaled, M. I. Khot, R. Aiyappa-Maudsley, T. Maisey, A. Pramanik, J. P. Tiernan, N. Lintern, E. Al-Enezi, S. H. Shamsuddin, D. C. Tomlinson, P. L. Coletta, P. A. Millner, T. A. Hughes and D. G. Jayne, *Nanoscale*, 2023, DOI: 10.1039/D3NR04118B.

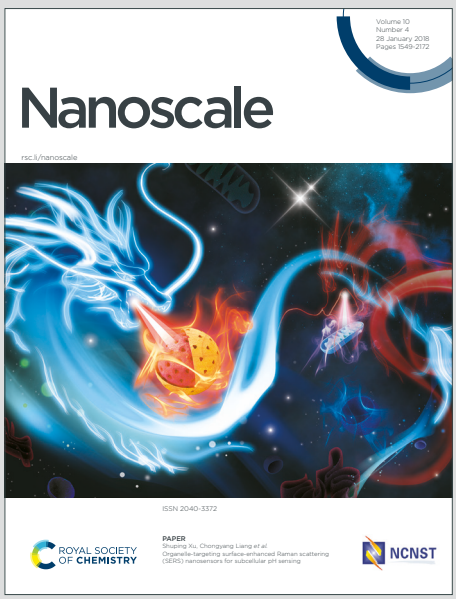

ROYAL SOCIETY OF CHEMISTRY

rsc.li/nanoscale

Title page

View Article Online
DOI: 10.1039/D3NR04118B

Title: Photoactive imaging and therapy for colorectal cancer using a CEA-Affimer conjugated Foslip nanoparticle.

Yazan S. Khaled[1]*, M. Ibrahim Khot[1], Radhika Aiyappa-Maudsley[1], Thomas Maisey[1], Arindam Pramanik[1], Jim Tiernan[1], Nicole Lintern[2], Eiman Al-Enezi[2], Shazana H. Shamsuddin[3], Darren Tomlinson[4], Louise Coletta[1], Paul A Millner[2], Thomas A. Hughes[5,6]*, David G. Jayne[1]*

[1]Leeds Institute of Medical Research, St James's University Hospital, Leeds, United Kingdom

[2]School of Biomedical Sciences, University of Leeds, Leeds, United Kingdom

[3]Department of Pathology, School of Medical Sciences, University Sains Malaysia, Malaysia

[4]School of Molecular and Cellular Biology, University of Leeds, Leeds, United Kingdom

[5]School of Medicine, University of Leeds, Leeds, United Kingdom

[6]School of Science, Technology and Health, York St John University, York, United Kingdom

*Joint lead authors

Corresponding author:

Dr. Yazan S. Khaled

Leeds Institute of Medical Research & School of Medicine

University of Leeds
Clinical Sciences Building
St James's University Hospital
Leeds, LS9 7TF
United Kingdom
Phone: +44 113 2065281
Fax: +44 113 2065281
Email: Y.Khaled@leeds.ac.uk

View Article Online
DOI: 10.1039/D3NR04118B

Keywords:
Antibody mimetic; cancer therapeutics; carcinoembryonic antigen; silica nanoparticle; photodynamic therapy; colorectal cancer; *in-vivo* targeted delivery.

Conflict of interest:
The authors declare no conflict of interest.

View Article Online
DOI: 10.1039/D3NR04118B

Abstract

Theranostic nanoparticles hold a promising strategy for simultaneous imaging and therapy in colorectal cancer. Carcinoembryonic antigen can be used as a target for these nanoparticles because it is overexpressed in most colorectal cancers. Affimers reagents are synthetic proteins capable to binding specific targets, with additional advantages over antibodies for targeting. We fabricated silica nanoparticles using a water-in-oil microemulsion technique, loaded them with the photosensitiser Foslip, and functionalised the surface with anti-CEA Affimers to facilitate fluorescent imaging and photodynamic therapy of colorectal cancer. CEA-specific fluorescent imaging and phototoxicity was quantified in colorectal cancer cell lines and a LS174T murine xenograft colorectal cancer model. Anti-CEA targeted nanoparticles exhibited CEA-specific fluorescence in LoVo, LS174T and HCT116 cell lines when compared to control particles ($p<0.0001$). No toxicity was observed in LS174T cancer mouse xenografts or other organs. Following photo-irradiation, anti-CEA targeted particles produced significant cell death in LoVo (60%), LS174T (90%) and HCT116 (70%) compared to controls ($p<0.0001$). Photodynamic therapy (PDT) at 24 h *in vivo* showed a 4-fold reduction in tumour volume compared to control mouse xenografts ($p<0.0001$). This study demonstrates the efficacy of targeted fluorescent imaging and PDT using Foslip nanoparticles conjugated to anti-CEA Affimer nanoparticles in *in vitro* and *in vivo* colorectal cancer models.

View Article Online
DOI: 10.1039/D3NR04118B

Introduction

Personalised surgery involves a tailored approach to the individual patient and the underlying disease. Up to 30% of colorectal cancer (CRC) patients undergoing curative surgical resection develop locoregional recurrence or distant metastases (1-3). Lymph node micrometastases and residual tumour cells are thought to be the main contributing factors. They are not detectable at surgery and can be easily missed during routine histopathological examination (4, 5). An accurate means of identifying positive lymph nodes (LN) intraoperatively would allow the radicality of surgery to be tailored to the biology of the primary cancer; lymph node positive cancers would undergo radical D3 lymphadenectomy, whereas lymph node negative cancers could be effectively treated by limited segmental resection. Reducing the radicality of surgery, whilst maintaining oncological efficacy, is important as the incidence of CRC is rising, particularly amongst the elderly population (6, 7).

Theranostics has emerged as a promising route for personalised cancer treatment, allowing real-time imaging of cancers and cytotoxic cell killing (8, 9). A theranostic photo-active nanoparticle would enable surgeons to visualise positive lymph nodes, tumour margins and distant metastasis intra-operatively, facilitating complete cancer eradication. Selective uptake of a photosensitiser (PS) by cancer cells allows fluorescent visualisation, whilst irradiation with a specific wavelength of light triggers cancer cell death due to generation of cytotoxic reactive oxygen species (ROS) (10-12). Photodynamic therapy is particularly attractive in cancer surgery, which is now mostly undertaken using laparoscopy. Changing the light wavelength delivered to the abdominal cavity to activate a PS is relatively straight forward.

One of few photosensitisers that is clinically approved for treatment of different cancers in Europe is meta-tetra(hydroxyphenyl)chlorin (mTHPC); commercially known

View Article Online
DOI: 10.1039/D3NR04118B

as Foscan® (13). mTHPC is characterised by its favourable absorption wavelength in the near infra-red region (652 nm) and high singlet oxygen quantum yield (14). In preclinical studies, the liposomal formulation of mTHPC, known as Foslip®, gave enhanced PDT efficacy and offered several advantages such as being non-immunogenic and biodegradable in addition to increasing drug solubility and tumour selectivity while reducing unwanted skin accumulation (15, 16). However, a lack of stability, with 60% of liposome destruction after 24 hours, is an obvious shortcoming (17-19). Leakage of the phospholipid membrane can be halted by coating the liposomes with a polymer net (20) or silica shell (21) and is widely used to stabilise the lipid bilayer (22). Silica based nanoparticles are attractive because of their compatibility with biological systems and transparency to light. Their degradation is enhanced by the increased ROS levels observed in the tumour microenvironment, facilitating delivery of the payload. Silica-based 'C dots' have recently been approved for Phase 2 clinical trials (23, 24). We have shown previously that carcinoembryonic antigen is a reliable tissue biomarker for colorectal cancer (25) and that our CEA antibody targeted NIR664 dye-doped silica nanoparticles allowed specific *in vivo* fluorescent imaging of colorectal cancer in a mouse model (26). However, antibody based drug targeting has its limitations, including high cost of production, stability, and batch-to-batch variation, which limit clinical translation (27, 28). Affimers are an attractive alternative with equivalent biorecognition characteristics to antibodies (29). The absence of cysteine residues in the Affimer scaffold allows the introduction of cysteine for site-specific conjugation to nanoparticles. Affimers are thermo- and pH-stable and easily expressed in prokaryotic cells (*E.coli*), thereby reducing the cost of production. We have recently shown that CEA-Affimers bind to cancer cells expressing CEA with high affinity and with K_D values in the nM range (30, 31).

View Article Online
DOI: 10.1039/D3NR04118B

The aim of this study was to develop a photoactive, theranostic nanoparticle for fluorescence tumour imaging and ablation. We report the first successful use of Affimer-targeted, silica-coated Foslip nanoparticles for fluorescent imaging and photodynamic therapy *in vitro* and in an animal CRC model.

View Article Online
DOI: 10.1039/D3NR04118B

Results

Synthesis and characterisation of Affimer tagged silica coated Foslip nanoparticles

We aimed to synthesise silica coated Foslip nanoparticles to target colorectal cancer cells using anti-CEA Affimers as bioreceptors. Silica coating formation was achieved by a hydrolysis process of TEOS, according to protocols published in the literature (32, 33). The precipitation of silica on the surface of Foslip resulted in the formation of a spherical core-shell-like structure, as visualised by scanning electron microscopy (**Figure 1A**), with a mean diameter of 140 nm (±1 nm SEM) (**Figure 1B)**. Encapsulation of Foslip was demonstrated by absorption and fluorescence emission spectra of the synthesised nanoparticles. Fluorescence of the nanoparticles was measured and recorded using a Cary Eclipse spectrofluorometer in water suspension, using specific Foslip excitation and emission wavelengths of 420 and 652 nm respectively (34). **Figure 1C** shows a typical spectrum for silica coated Foslip particles, along with a spectrum for Foslip alone, demonstrating that encapsulation does not alter the spectral properties. The efficiency of the encapsulation (EE) process was quantified by measuring the absorbance of Foslip with reference to a dose standard curve using a microplate reader (**Figure S1**). A typical nanoparticle sample containing 1 mg/ml of nanoparticles and 110 nM of Foslip correlated to Foslip EE of ~82.2 ± 2.1% (n=3). We also assessed the stability of nanoparticles in different conditions by measuring their fluorescence using a plate reader, as shown in **Figure 1D.** Particles remained highly fluorescent either in stock PBS at 4 ^{o}C (98.5%) or in PBS containing 10% (v/v) FBS at 37 ^{o}C (97.0%) for 48 h, when compared to freshly synthesised NPs, after which the signal reduced most likely due to leakage of mTHPC; **Figure S2**.

View Article Online
DOI: 10.1039/D3NR04118B

Despite this limitation, the NPs were able to achieve their target imaging and cytotoxicity in less than 48 h as shown in following results.

Next, we selected two different anti-CEA Affimers (based on protein yield) to provide polyclonal targeting of the CRC-antigen CEA, and as a control, an anti-myoglobin (Myo) Affimer. The anti-myoglobin Affimer was used as a negative control because colorectal cancer cells do not express this human cardiac muscle-related protein. Tris (2-carboxyethyl) phosphine (TCEP) reduced anti-CEA and anti-Myo Affimers were purified using Ni^{2+}-NTA resin (**Figure S3, Table ST1**) and prepared for conjugation. The hetero bifunctional cross-linker sSMCC (sulfosuccinimidyl 4-(N-maleimidomethyl) cyclohexane-1-carboxylate) was then used to link the free Affimer sulfhydryl group to the aminated nanoparticle surface (provided by the salinisation agent, 3-aminopropyl triethoxysilane (APTES)) as shown in **Figure S4**.

Quantification of Affimer amount bound to NPs comprised two main parts; (i), cleavage of disulfide bond crosslink between Affimer and NPs, and (ii), quantification of the Affimers concentration. The Affimer-tagged NPs were prepared at 1 mg/mL concentration and reducing agent 2-mercaptoethanol was used to break the thiol-maleimide conjugation and free the Affimers. Free Affimers were recovered from the supernatant and the concentration was measured using a calibration curve for NanoOrange® protein; **Figure 1E.** Knowing the estimate number of NPs per mL (~ 8.5 x 10^7), the number of Affimers immobilised on each NP was estimated at 570 +/- 110 Affimer/NP.

Dynamic light scattering (DLS), showed monodispersed particle peaks at 148 nm ($\pm$ 11 nm) and reassuringly, CEA-Fos-NPs and Myo-Fos-NPs showed almost identical size distributions; **Figure 1F**. The mean zeta potential of the silica coated Foslip exhibited a negative surface charge (-15.6 mV) whereas aminated NPs exhibited a

positive surface charge (27.9 mV). The surface charge of the Affimer-tagged NPs shifted back to a more neutral charge state (2.8 mV) indicating successful conjugation. The size distribution, zeta potential and polydispersity index (PDI) of NPs derivatives is shown in **Table 1**.

View Article Online
DOI: 10.1039/D3NR04118B

View Article Online
DOI: 10.1039/D3NR04118B

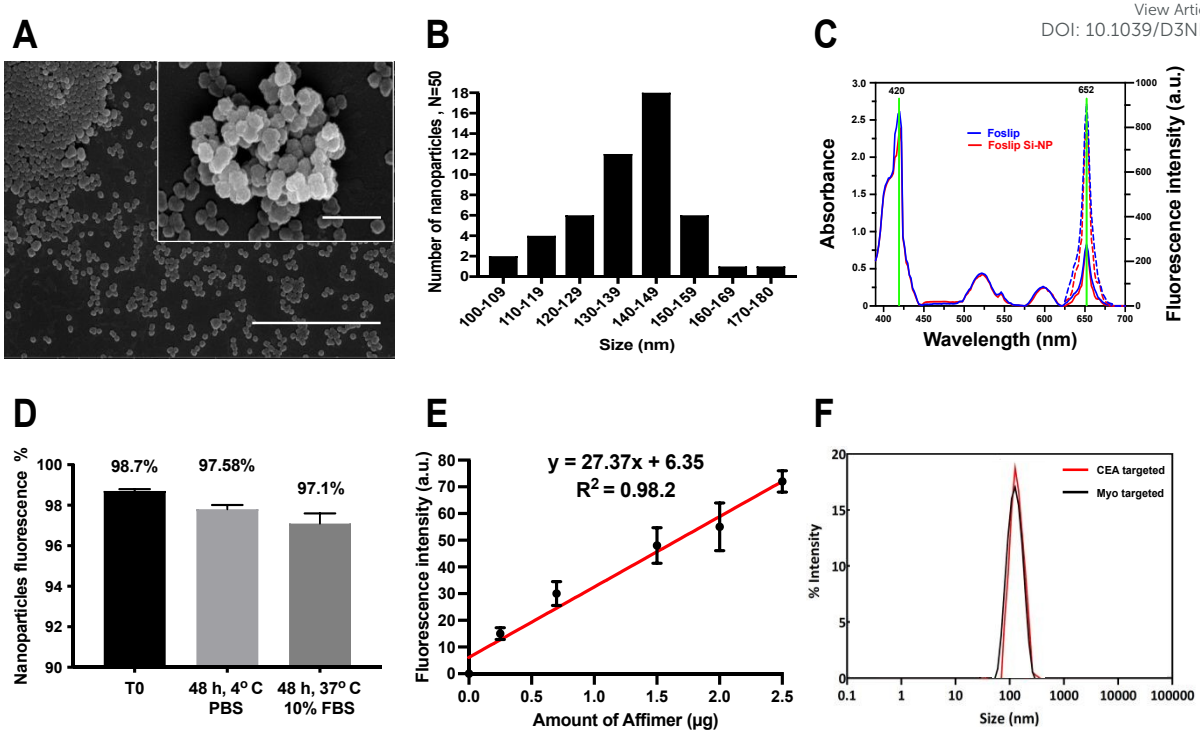

Table 1. Size distribution, zeta potential and PDI data of NP derivatives.

Batch	Z-average hydrodynamic diameter (nm)	Zeta potential (mV)	PDI
Si-Fos-NP	138 (±4 nm)	-15.6 (± 4.2 mV)	0.21
Aminated Si-Fos-NP	140 (±2 nm)	27.9 (± 12.4 mV)	0.24
CEA/Myo-Fos-NP	148 (±1 nm)	2.8 (± 1.1 mV)	0.19

Abbreviations: Si-Fos-NP, silica coated Foslip nanoparticle; CEA/Myo-Fos-NP, CEA or Myo Affimer tagged silica coated Foslip nanoparticle; PDI, polydispersity index.

Figure 1. *Characterisation of silica coated Foslip NPs*. (A), SEM image shows a spherical structure of NPs with size around 140 nm. The scale bars represent 1 µm and 500 nm respectively for the whole view and the magnified view. (B), The size distribution is shown with particle diameters being binned into 10 nm intervals. (C), UV absorption spectra for Foslip alone (▬), silica coated Foslip NPs (▬) and fluorescence spectra for Foslip alone (▬ ▬ ▬) and silica coated Foslip NPs (▬ ▬ ▬). D), Stability of Affimer tagged NPs monitored by fluorescence intensity under different condition using spectrofluorometer: the freshly prepared particles (T0); the sample stored for 48 h at 4 °C in PBS; and the sample incubated at 37 °C in 10% FBS for 48 h. Data show mean from 3 biological experiments (SEM, n=3). (E), A calibration curve of fluorescence intensity for NanoOrange dye with increasing dose of Affimer concentration. Data show mean from 3 biological experiments (SEM, n=3). (F), Affimer tagged NPs size as determined by DLS.

View Article Online
DOI: 10.1039/D3NR04118B

CEA-Fos-NPs enabled selective fluorescent imaging and cytotoxicity in colorectal cancer cells lines.

We aimed to assess the fluorescence and PDT effect on three colorectal cancer cell lines (LoVo, LS174T and HCT116) and a control, CEA-negative non-cancer cell line (HEK293) when incubated with CEA-Fos-NPs. We have previously reported that LoVo cells show high CEA expression, LS174T cells moderate to high CEA expression, HCT116 cells low CEA expression, and HEK293 cells no expression of CEA (26). Anti-CEA or Myo- Affimer tagged nanoparticles (1 mg/mL) were incubated with colorectal cancer and control cell lines for 24 h then imaged using confocal microscopy and cell-specific fluorescence was quantified. CEA-Fos-NPs produced more intense tumour-specific targeting, with anti-CEA targeted nanoparticles showing 9.5-, 10.2- and 3.5-fold greater fluorescence than Myo-Affimer targeted nanoparticles in LoVo, LS174T and HCT116 cells respectively ($p<0.0001$) as shown in **Figure 2A**. Importantly, CEA-Fos-NPs did not produce any significant fluorescence intensity in the control cell line HEK293, suggesting that that the anti-CEA Affimer targeted silica nanoparticles were specific to CEA expressing cells and likely to prevent unwanted accumulation in normal tissues, thereby reducing side effects. Representative confocal microscopy images showed fluorescence in tumour cells at 24 h that correlates with CEA expression data in the literature (**Figure 2B**). In order to assess the dose- and time-effect on cellular fluorescence, cells were incubated with 1 or 2 mg/mL nanoparticles for 4 and 24 h. After incubation, the cells were washed and fresh nanoparticle-free media was added for an additional 20 h (4+20 h) or 24 h (24+24 h). Spectrofluorometer evaluation showed that LoVo cells had significantly higher fluorescent signal with CEA-Fos-NPs than other cell lines ($p<0.02$), followed by LS174T and HCT116 cells, in a dose and time dependent manner (**Figure 2C**). Cellular uptake was seen as early as

View Article Online
DOI: 10.1039/D3NR04118B

4 h but the difference between the single time points was most obvious at 24 and 24+24 h in all cancer cell lines. Although fluorescence was still present in cells after 24 h incubation, the mean fluorescence intensity at 24+24 h was greater than 24 h ($p=0.01$), indicating that cellular uptake was also time dependent. The mean fluorescence in HEK293 cell lines was almost identical at 4+20 h and 24 h ($p>0.9$) whilst in the colorectal cell lines a significant difference was observed between these two time points ($p<0.001$), highlighting that the anti-CEA Affimer increased the selectively for cancer cells.

Next, we assessed the internalisation and co-localisation characteristics of NPs in LoVo and LS174T cells. For the purpose of this experiment, we synthesised silica NPs tagged with fluorescein isothiocyanate (FITC) and CEA or Myo-Affimer. NPs (1 mg/mL, 150 nm ($\pm$ 12 nm)) were incubated with cells for 1, 4 and 24 hours then imaged by fluorescent microscopy to track internalisation. To determine the subcellular localisation of NPs, we subsequently stained cells with lysotracker deep red. Based on fluorescent microscope images, CEA-FITC-NPs were internalised in LoVo and LS174T as early as 1 h whereas Myo-FITC-NPs were negligibly internalised. The CEA-targeted NPs predominantly accumulated into the cytoplasm, with some lysosomal localisation as shown in **Figure 2D**, where the lysotracker (red) and the nanoparticles (green) were co-localised (yellow).

View Article Online
DOI: 10.1039/D3NR04118B

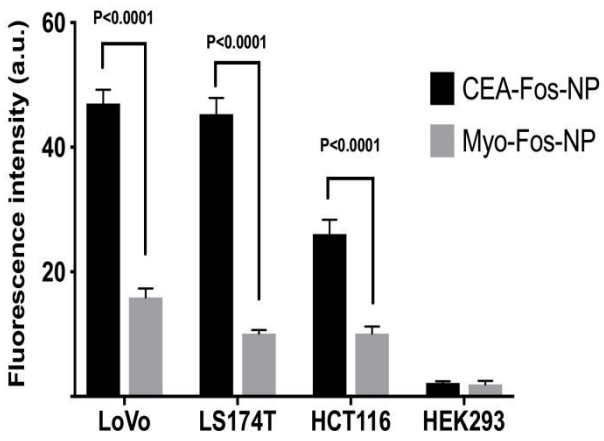

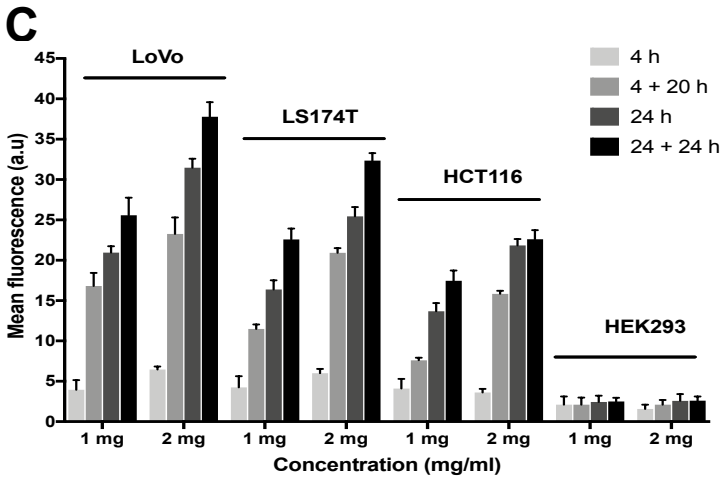

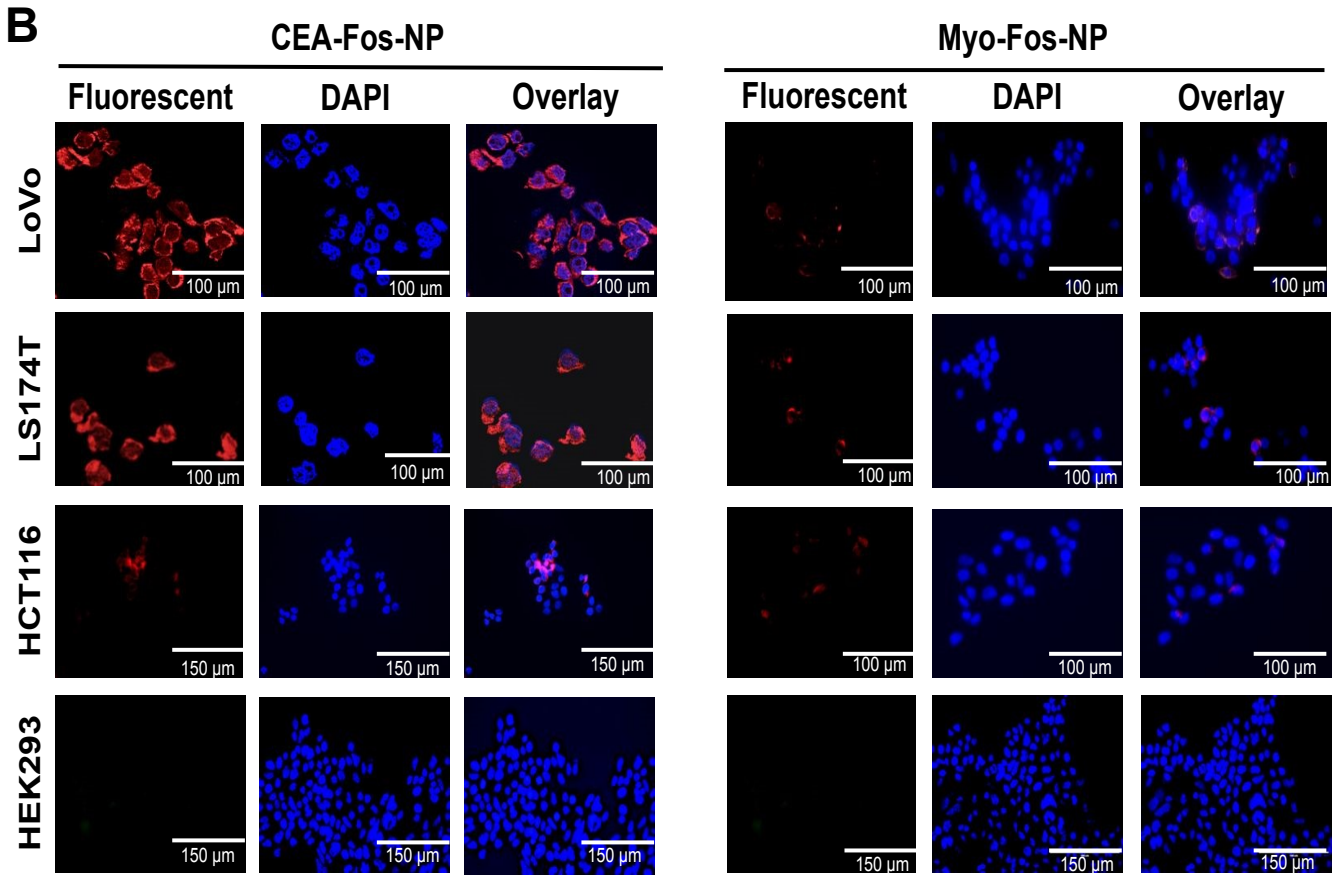

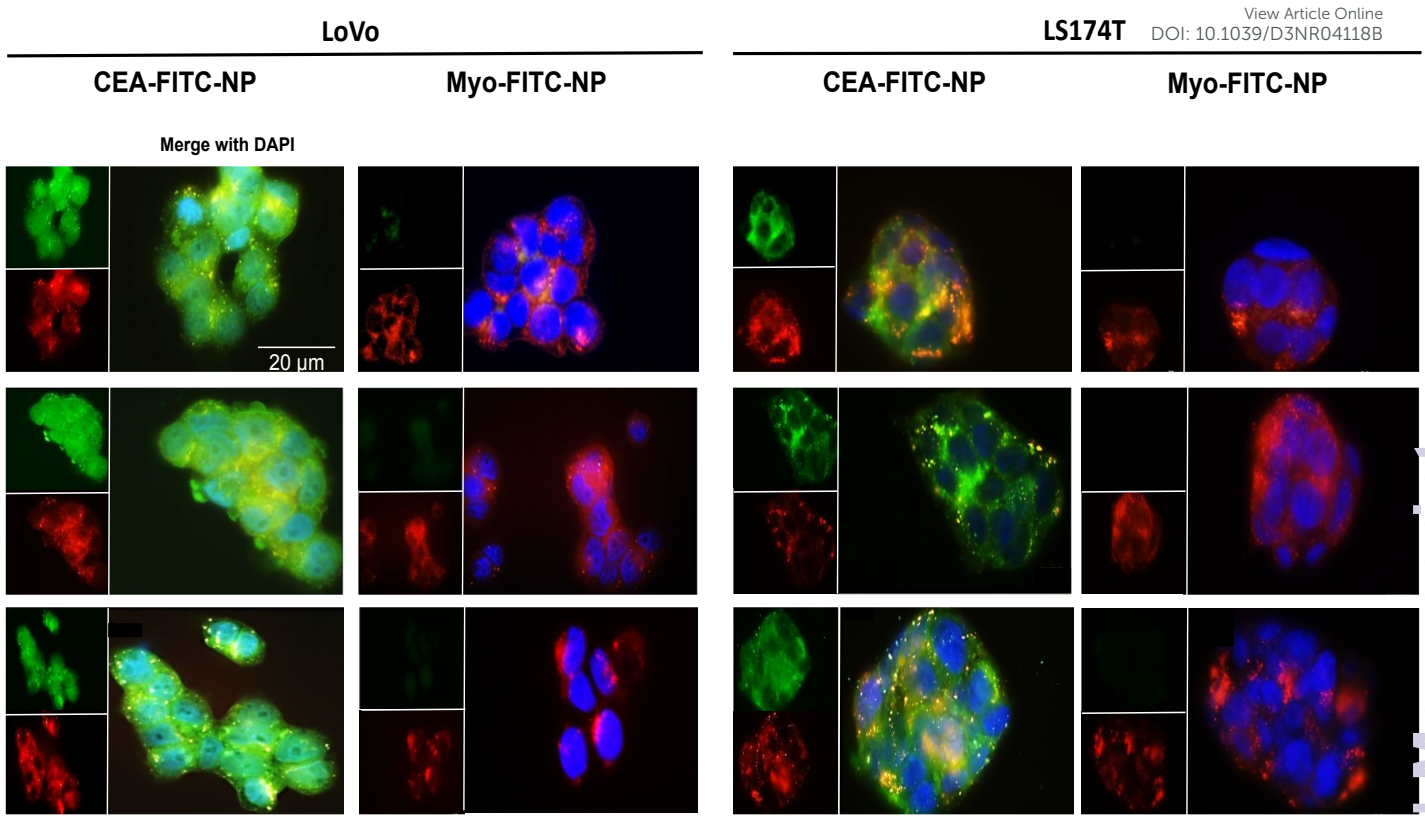

Figure 2. *CEA-Fos-NPs enabled targeted fluorescent imaging of CRC cells*. (A) Comparing the fluorescence intensity in CRC cancer cells when incubated with either nanoparticles conjugated to CEA-Fos-NPs or Myo-Fos-NPs for 24 h. Data denote fluorescence mean from 3 biological experiments (SEM, n=3). Significance was tested using unpaired t-tests. (B) Representative confocal images of LoVo, LS174T, HCT116 and HEK293 cells right after 24 h incubation with CEA-Fos-NPs or Myo-Fos-NPs. (C) Cellular uptake of CEA-Fos-NPs in CRC and control cell lines at different time points and nanoparticle concentrations. Cells were incubated with 1 or 2 mg/mL of anti-CEA targeted nanoparticles for 4 and 24 h. After incubation, the cells were washed and fresh nanoparticle-free media was added for an additional 20 h (4+ 20 h) and 24 h (24+24 h). Data denote fluorescence mean from 3 biological experiments (SEM, n=3). (D) Fluorescence images of CEA-FITC-NPs internalised into cytoplasm and lysosomes of LoVo and LS174T. Images show FITC from NPs (green, top left), lystotracker staining of lysosomes (Red, bottom left) and merged DAPI fluorescence of NPs and lysosomes (yellow, magnified). Scale bar is 20 µm for all images.

View Article Online
DOI: 10.1039/D3NR04118B

Next, we assessed the dark cytotoxicity of CEA-Fos-NPs against colorectal cancer cells. Cells were incubated with CEA- or Myo-Fos-NPs at high concentration of 3 mg/mL for 24 h and 24+24 h then washed and kept in nanoparticle-free media followed by MTT assay quantification of cellular viability. Cells were kept in the dark during incubation periods. Affimer tagged Fos-NPs did not affect the survival of all cell lines when exposed at high concentrations of 3 mg/mL for 24 h, which is much higher than that used to achieve cell-specific fluorescence and cellular uptake in previous experiments. Similarly, the MTT assay showed that the number of metabolically active cells at 24+24 h after exposure to nanoparticles was not reduced relative to controls (**Figure S5**).

We assessed the light dose effect on cell survival to ensure that any cytotoxic effect was Foslip-mediated only. Cells were incubated with CEA-Fos-NPs at various concentrations for 24 h, washed and incubated with fresh media, and immediately incubated in the dark (0 J/cm^2) or photo-irradiated with light doses from 0.15 to 0.675 J/cm^2. Cells were then kept in nanoparticle-free media for an additional 24 h followed by assessment of cell viability by MTT assay.

In all the cancer cells, significantly reduced viability of cells was observed that was dependent on light dose, and on nanoparticle dose ($p<0.0001$; **Figure 3A-C**), with no reduction in viability in the absence of nanoparticles at any light dose. For example, more than 80% reduced viability was seen at the highest doses of nanoparticles after 0.45 J/cm^2 irradiation. By contrast, HEK293 cells showed no reduction in viability at any dose of nanoparticles below 0.6 J/cm^2 (**Figure 3D**); at 0.6 J/cm^2 and above, HEK293 cells showed light-induced toxicity that was independent of the presence of nanoparticles suggesting that these cells were more sensitive to the light alone than

View Article Online
DOI: 10.1039/D3NR04118B

the cancer cells. Therefore, light dose at 0.45 J/cm^2 was considered as the cut-off point for safe photo-irradiation of cells in the next experiment.

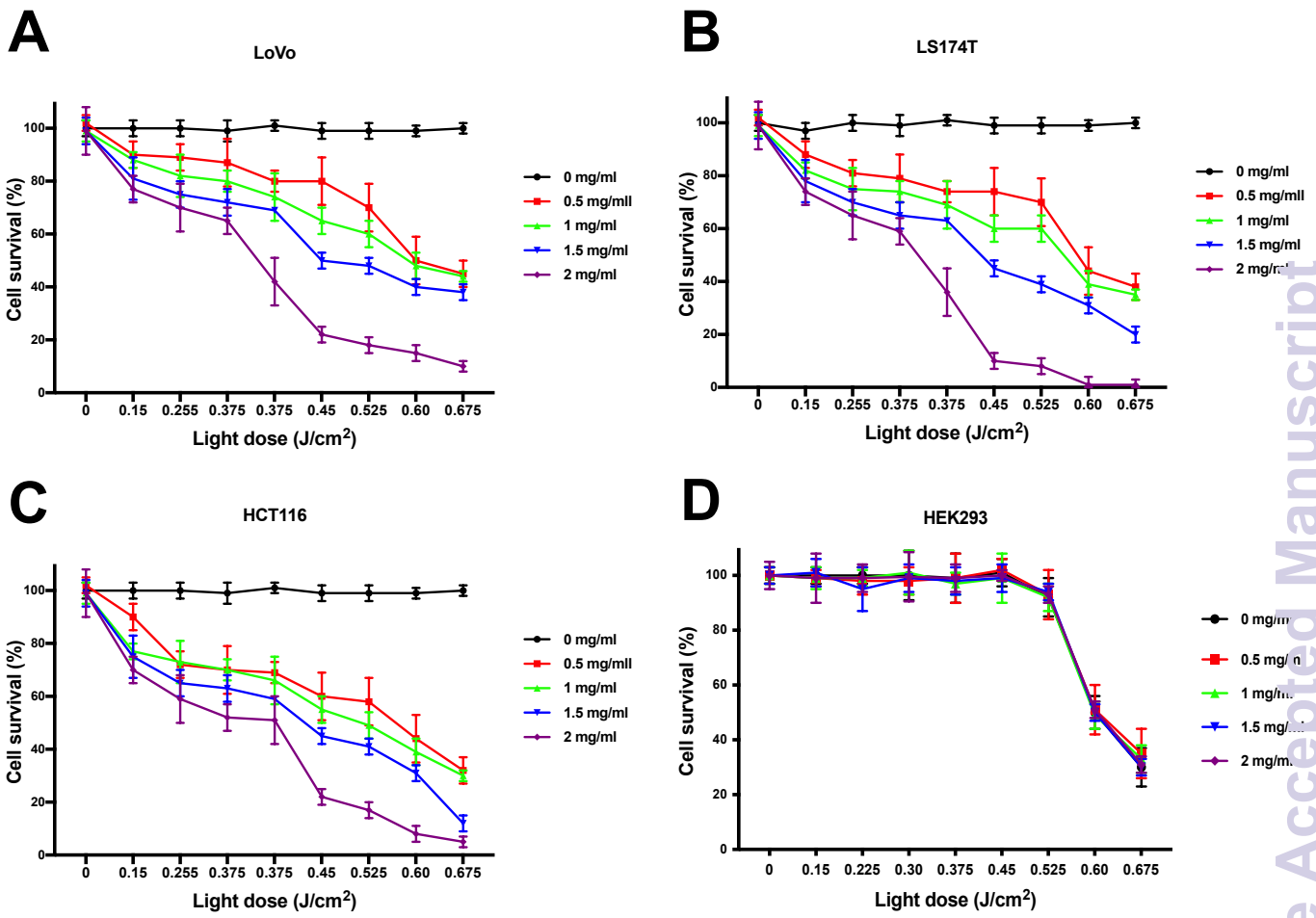

Figure 3. *Light dose and nanoparticles concentration effect in CRC cells*. (A-D) Cells were incubated with various concentrations of CEA-Fos-NPs for 24 h then photo-irradiated with 0.15 – 0.675 J/cm^2 of 600-700 nm. Cells viability was quantified using MTT assay. Data show mean cells viability from 3 biological experiments (SEM, n=3).

View Article Online
DOI: 10.1039/D3NR04118B

Next, we assessed the phototoxicity efficacy of CEA-Fos-NPs in killing cancer cells when photo-irradiated with the optimum light dose of 0.45 J/cm^2. Cells were incubated with CEA-Fos-NPs or Myo-Fos-NPs at various concentrations for 24 h, washed and incubated with fresh media, and immediately photo-irradiated with light doses of 0.45 J/cm^2 followed by MTT assay assessment as described previously. As shown in **Figure 4A**, at 0.45 J/cm^2 light dose a significant reduction in cell survival was observed in LoVo, LS174T and HCT116 cells when compared to control HEK293 cells ($p<0.0001$). The reduction in cell survival measured at 24 h after irradiation with an optimum light dose of 0.45 J/cm^2 was dose dependent. At 2 mg/mL CEA-Fos-NPs concentration, significant cell death was observed in LoVo (60%), LS174T (90%) and HCT116 (70%) when compared to HEK293 (0%); $p<0.0001$. Importantly, no cellular toxicity was observed when cells were treated with increasing dose of the control anti-myoglobin Affimer nanoparticles at 0.45 J/cm^2 (**Figure 4B**). Interestingly, the PDT induced cellular toxicity did not correlate with the fluorescence intensity seen in the respective cell lines as shown earlier in **Figure 2**. As cell density per well may impact the overall PDT efficacy, we attempted to standardise this variable by measuring cell viability per 1000 cells per well. Following PDT, cells were trypsinised and stained with trypan blue and the number of viable cells per 1000 cells per well was calculated (**Figure S6**). The data show when cell numbers was standardised per well, LoVo cells viability dropped to ~ 30 %. Importantly, the variation in response to PDT appeared to correspond to the degree of differentiation of the cell line suggesting that tumour cell biology and genetic differences may be associated with variations in cellular pathways and overall sensitivity to PDT.

The DCFDA assay was performed to study the cell death mechanism following PDT to mimic the experiments in which cell viability was assessed using the MTT assay.

View Article Online
DOI: 10.1039/D3NR04118B

DCF fluorescence was observed using confocal microscope. The assay showed strong fluorescence in all cancer cells treated with CEA-Fos-NPs but not with Myo-Fos-NPs or in control cells (**Figure 4C**). The results support the hypothesis that the cytotoxic effect seen in the PDT experiment was Foslip mediated via ROS generation. Collectively, Foslip-loaded silica nanoparticles conjugated to anti-CEA Affimers allowed tumour cell-specific fluorescence and photodynamic therapy *in vitro*.

View Article Online
DOI: 10.1039/D3NR04118B

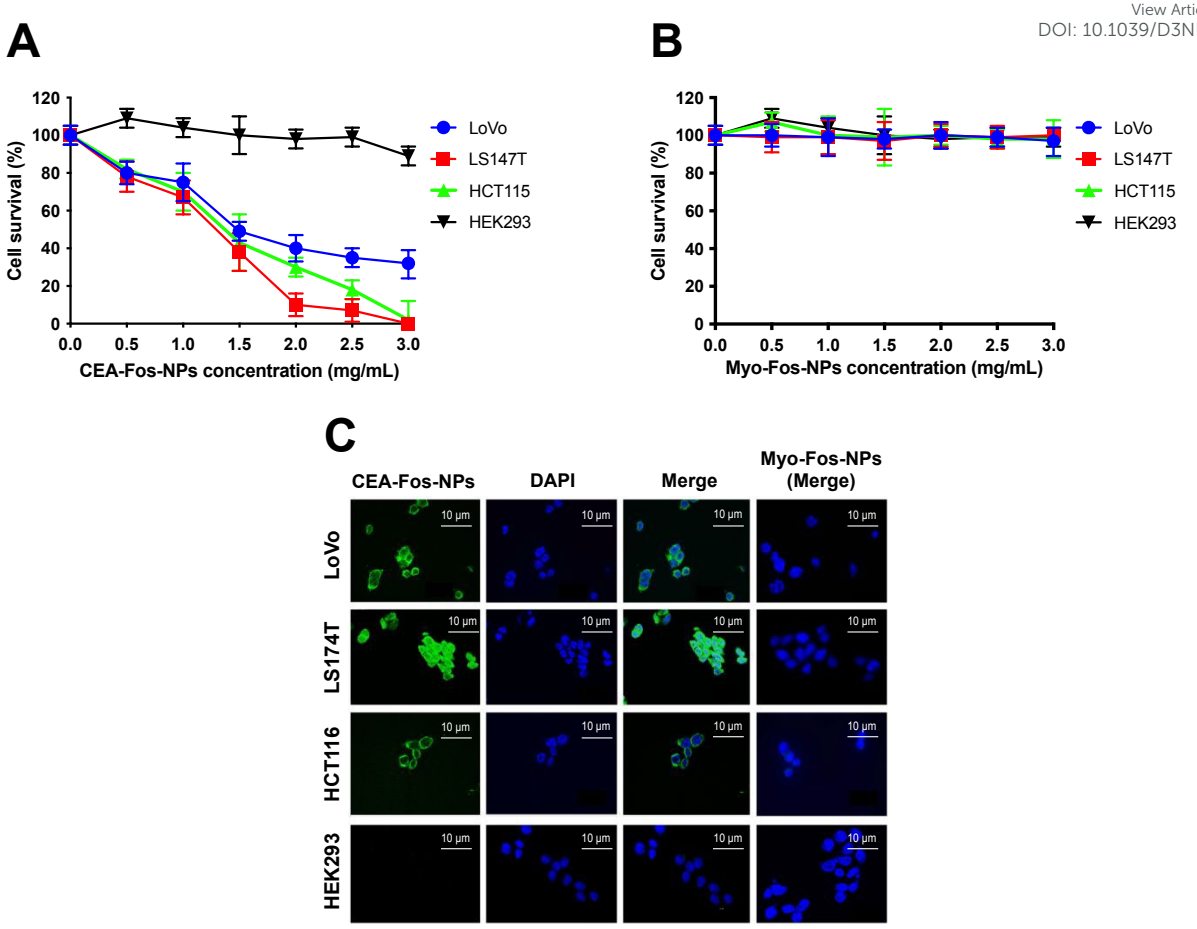

Figure 4. *CEA-Fos-NPs enabled targeted PDT in CRC cells*. Cells were incubated with various concentrations of CEA-Fos-NPs or Myo-Fos-NPs respectively for 24 h then photo-irradiated with 0.45 J/cm^2 of 600-700 nm. Cells viability was quantified using MTT assay. Data show mean cells viability from 3 biological experiments (SEM, n=3). (C), Representative confocal images of ROS detection in cells following PDT post-incubation with nanoparticles at 2 mg/mL concentration and 0.45 J/cm^2 light dose are shown. Cells were incubated with PBS containing 10 mM DCFDA for 30 minutes in a CO_2 incubator then washed with PBS. DCF fluorescence observed in cells and their respective DAPI staining are shown. Confocal images of ROS detection showed DCF fluorescence in cancer cells treated CEA-Fos-NPs but not with Myo-Fos-NPs.

Theranostic application of CEA-Fos-NPs in LS174T xenograft model of colorectal cancer

We next assessed the theranostic potential of CEA-Fos-NPs in a clinically relevant mouse xenograft model of colorectal cancer. The tumour growth pattern of LS174T xenograft is shown in **Figure S7**. Nanoparticles were suspended in sterile PBS at 2 mg/mL concentration and 150 µL of nanoparticles injected into the tail vein of mice. Two groups of five mice were injected with either CEA-Fos-NPs (n=5) or control Myo-Fos-NPs (n=5) and imaged at 6, 24, 30 and 48 h. For better understanding of the biodistribution and fate of the nanoparticles, one mouse from each group was sacrificed after imaging at each time point and organs were harvested then imaged *ex vivo*. The background fluorescence point was set high to eliminate the hepato-biliary fluorescence and ensure that any fluorescence seen in the xenograft was a real signal. Tumour-specific fluorescence was seen in the xenografts of mice that were injected with CEA-Fos-NPs as shown in **Figure 5A**. No fluorescent signal was seen in any of the mice that were injected with Myo-Fos-NPs. The fluorescent signal was seen as early as 6 h, peaked at 24-30 h and remained in the xenograft at 48 h. When background fluorescence was set to a lower point (~ 50 x 10^6 (p/s/cm^2/sr) / (µW/cm^2)), Foslip loaded nanoparticles exhibited a similar biodistribution to our previously published report on NIR664-dye-doped silica nanoparticles (26); **Figure 5B and 5C.** Liver fluorescence was evident at 6 h in all mice (mean 59.1 x 10^6 (p/s/cm^2/sr) / (µW/cm^2)) and increased at 24 h (85.8 x 10^6 (p/s/cm^2/sr) / (µW/cm^2)). Hepatic localisation was confirmed by *ex vivo* imaging of isolated organs. There was no significant difference in liver fluorescence between mice injected with control particles and those injected with anti-CEA Affimer targeted particles at any time point; **Figure S8**.

View Article Online
DOI: 10.1039/D3NR04118B

Fluorescence in the CEA-targeted tumours was significantly greater than Myo-targeted tumours at all time points ($p<0.0001$). Mean tumour fluorescence increased from 6 h (mean 0.55 x 10^7 (p/s/cm^2/sr) / (μW/cm^2)) to 30 h (mean 9.415 x 10^7 (p/s/cm^2/sr) / (μW/cm^2)); **Figure 5D**. The fluorescence ratio, which was defined as the fluorescence of the tumour site over the fluorescence of normal tissue, at 6, 24, 30 and 48 h was 21, 88, 95 and 85 respectively. No tumour fluorescence, above background, was seen in mice injected with Myo-Fos-NPs.

Tumour tissue, and other organs, were harvested and imaged *ex vivo*. Tumour fluorescence was only detected in xenografts from mice injected with CEA-Fos-NPs, as shown in **Figure 5E**. Importantly, the *ex vivo* imaging of the CEA-targeted xenografts showed fluorescence within the core of the xenograft, suggesting that the nanoparticles accumulated within the tumour microenvironment. To confirm this, confocal imaging was performed on histological sections from a xenograft of a mouse injected with CEA-Fos-NPs and Myo-Fos-NPs; **Figure 5F**. The xenograft showed fluorescent signal within the tumour (section taken through the middle of the xenograft) whilst no fluorescence was seen in the control xenograft, suggesting directed-nanoparticle delivery to the tumour site.

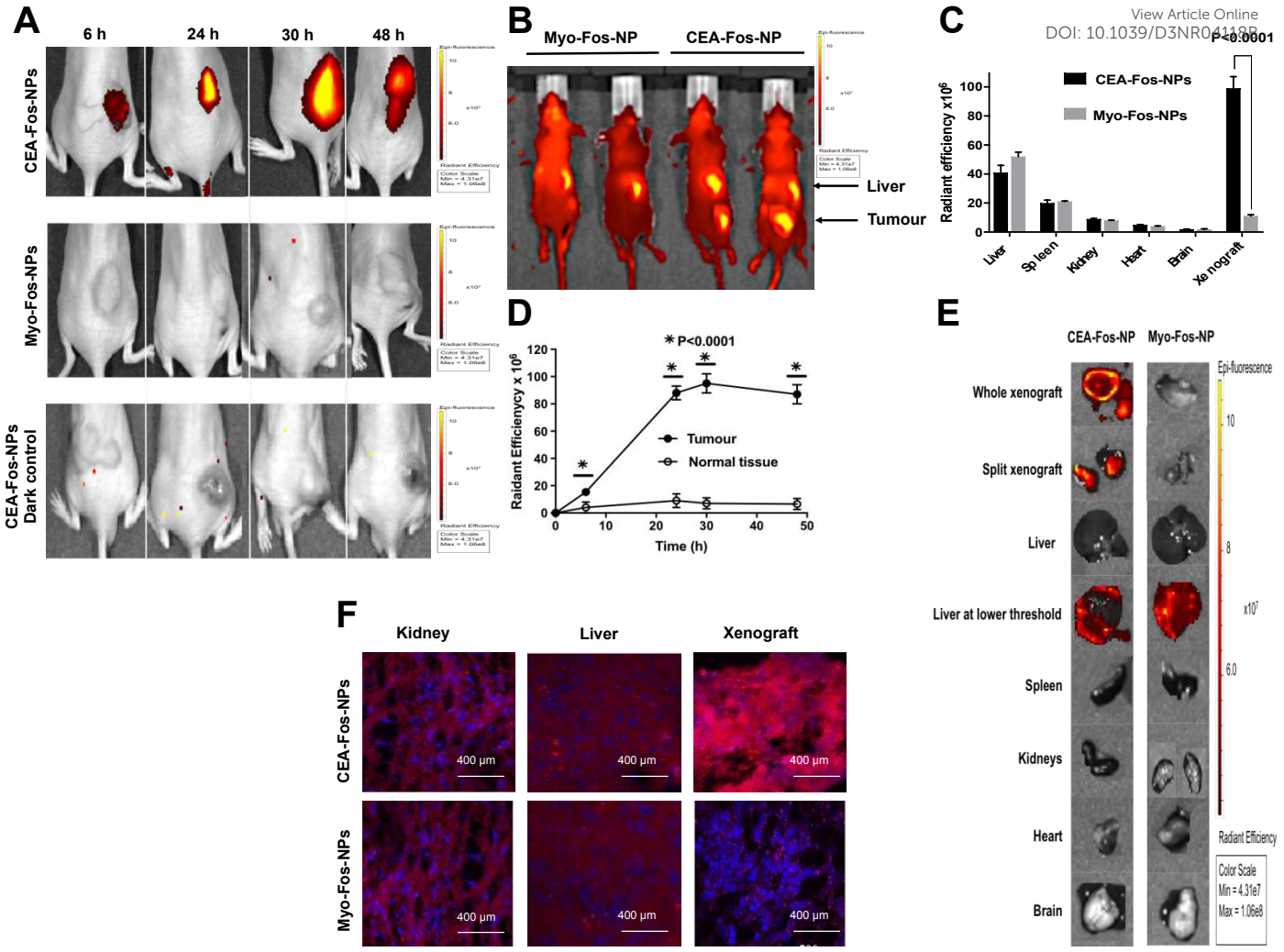

459

460 Figure 5. *CEA-Fos-NPs enabled targeted fluorescent imaging of CRC in vivo.* (A)
461 Representative *in vivo* fluorescence activation of CEA-targeted versus control NPs in
462 LS174T xenograft model at 6, 24, 30 and 48 h after intravenous injection with 150 µL
463 (2 mg/mL), n=5. Colour scale bar: minimum = 4.31 x 10^7 and maximum = 1.06 x 10^8
464 (p/s/cm^2/sr) / (µW/cm^2). (B) Fluorescence *in vivo* biodistribution of CEA-targeted and
465 control NPs at 24 h post NPs injection. (C), NPs biodistribution quantified using IVIS
466 with excitation filters at 615 - 665 nm and 8 s exposure time. Data show fluorescence
467 mean (SEM, n=5). (D) Data are mean tumour fluorescence for *in vivo* xenografts for
468 mice injected with CEA-Fos-NPs and Myo-Fos-NPs (SEM, n=5). Normal tissue
469 represents skin. (E) Representative *ex vivo* fluorescence images of the excised organs
470 and xenografts from CEA-targeted and control dosed mice at 24 h post injection. Liver
471 at lower threshold = (~ 50 x 10^6 (p/s/cm^2/sr) / (µW/cm^2)). Colour scale bar: minimum =
472 4.31 x 10^7 and maximum = 1.06 x 10^8 (p/s/cm^2/sr) / (µW/cm^2). (F) Fluorescence
473 histology images of kidney, liver and tumour xenograft from mice injected with CEA-
474 Fos-NPs and Myo-Fos-NPs 48 h after injection using confocal microscopy.

View Article Online
DOI: 10.1039/D3NR04118B

Having observed significant accumulation of CEA-Fos-NPs in colorectal tumours, we next wished to test whether they could mediate efficient PDT activity *in vivo*. A further *in vivo* experiment was performed: xenograft tumours were established as before and animals were split randomly into four groups (each n=5). Two groups were treated with CEA-Fos-NPs and with Myo-Fos-NP as previously then subjected to PDT. Two control groups were treated with CEA-Fos-NPs or Myo-Fos-NP and received no PDT. PDT, given 24 h post-delivery of NPs, consisted of trans-cutaneous laser irradiation (650 nm, 60 mW/cm^2, 50 J/cm^2, 14 min). The PDT efficacy was evaluated by tumour volume measurements and postmortem histopathological analysis. To eliminate the possibility of laser-induced thermal ablation and cell death in xenografts, thermal imaging videos were recorded for 1 min at 0 min, 7 mins and 14 mins during treatment for each mouse and we found no noticeable increase in surface temperature during laser treatment (**Figure S9**). The CEA-targeted PDT group displayed ~ 4-fold decrease in tumour volume when compared to Myo-targeted PDT group at day 5 (0.24 vs 3.15 median; P<0.001) whilst mice weights remained unchanged in all groups; **Figure 6A-C**. Importantly, there was no reduction in tumour volume in any of the dark control groups. Histological analysis showed condensed nuclei and loss of cell structure in tumour xenografts of CEA-targeted PDT, which was not observed in control groups; **Figure 6D**. TUNEL assay revealed dense staining (brown) at the site of DNA fragmentation in CEA-Fos-NPs PDT xenografts in keeping with significant tumour cell apoptosis (64 $\pm$ 2.3%), whilst the controls showed methyl green of normal cells indicating no tumour apoptosis (2 $\pm$ 0.1% for Myo-Fos-NPs, 1.8 $\pm$ 0.5% and 1.3 $\pm$ 0.3% for PDT-negative controls) (**Figure 6E)**. Overall, the results demonstrate the high selectivity and accuracy of CEA-targeted PDT to colorectal tumour xenografts.

View Article Online
DOI: 10.1039/D3NR04118B

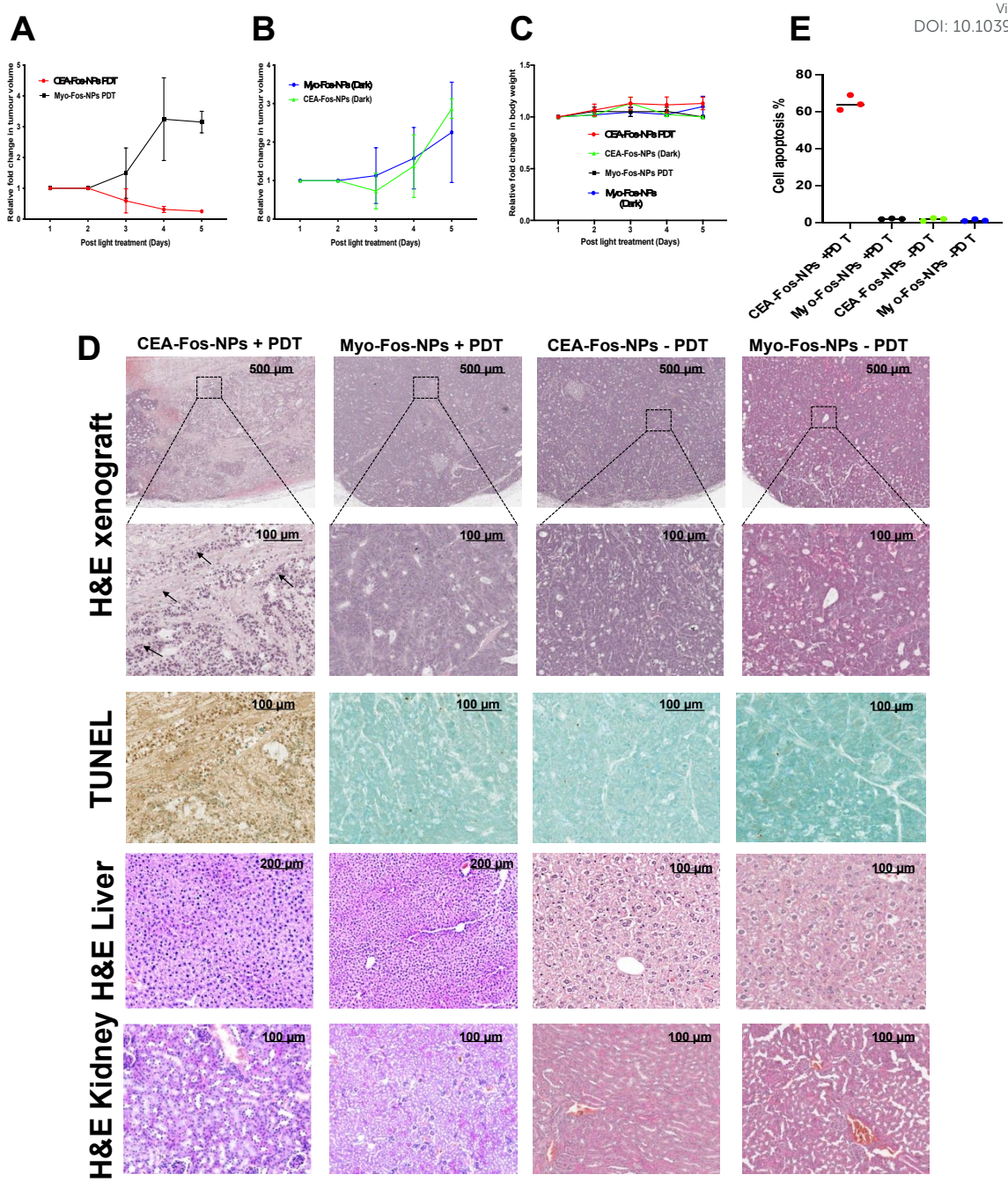

Figure 6. *CEA-Fos-NPs enabled targeted PDT of CRC in vivo.* (A) Tumour growthcurves of PDT groups over the treatment period until mouse sacrifice (SEM, n=5). (B), Tumour growth curves of control dark groups over the treatment period until mouse sacrifice (SEM, n=5). (C) Body weight curves of different groups over the treatment period until mouse sacrifice, (SEM, n=5). (D) Representative images of histological analyses of tumour sections (H&E and TUNEL staining), liver and kidney (H&E) at day 5 post treatment. Black arrows point to condensed nuclei and loss of cells structure. (E) Quantitative analysis of TUNEL positivity out of whole tumour region in the four groups (n = 3).

View Article Online
DOI: 10.1039/D3NR04118B

Discussion

Developing a targeted nanoparticle against a specific tissue to produce a reliable molecular probe remains challenging. Several studies have demonstrated improved delivery when a nanoparticle is actively targeted to CEA in colorectal cancer cells using site specific reagents such as antibodies, antibody-fragments, aptamers, peptides and nanobodies (35-39). To date, anti-CEA antibody has shown the most promising targeting bioreceptor in colorectal murine models but translation to clinical application was complicated by the immunogenicity and the clearance from bloodstream, both owing to binding of Fc receptor–containing entities to the antibody Fc region (40). In addition, antibody size (~150 kDa) makes cell penetration difficult. Tiernan *et al* (2015) were the first to show specific tumour fluorescent imaging using NIR669-doped silica nanoparticles (mean diameter of 65 nm) in LS174T murine xenograft mouse model (26). They immobolised monoclonal anti-CEA antibody to the surface of the nanoparticle using PAMAM dendrimer. Conjugation of anti-CEA Affimer carried out with sSMCC, as used here, showed strong tumour-specific targeting in the same animal model. However, anti-CEA Affimer targeted xenografts exhibited higher fluorescence mean 9.415 x 10^7 (p/s/cm^2/sr) / (μW/cm^2) vs 4.74 x 10^7 (p/s/cm^2/sr) / (μW/cm^2) and a similar biodistribution but with notably lower liver uptake. In keeping with our findings, Pramanik *et al* (2022) have shown that anti-CEA Affimer tagged cubosomes, loaded with copper acetylacetonate as a model drug, actively targeted LS174T colorectal cancer cells *in vivo* (41). The authors showed preferential accumulation in colorectal cancer mouse xenografts, while maintaining low nonspecific absorption and toxicity in other organs. Owing to their small size (~12 kDa), controlled orientation on the surface of nanoparticles and their high affinity to CEA expressing cells ($K_D = 15.3 \pm 0.37$ nM and 34.4 ± 16 nM for the two Affimers

View Article Online
DOI: 10.1039/D3NR04118B

tested) (30), anti-CEA Affimers are expected to achieve important advances in CEA-targeting nano technologies. Despite the huge potential of new tools, targeting the CEA biomarker, uptake of research into CEA-targeting systems to enhance the efficiency of colorectal cancer targeting has been modest.

High accumulation and penetration of anti-cancer drugs into the inner parts of the tumour tissues are required to efficiently eradicate malignancies. Our data showed that anti-CEA Affimer targeted nanoparticles allowed significant Foslip-mediated localisation in tumour cells and photodynamic therapy *in vitro* and *in vivo* when compared to control nanoparticles. Reports on targeted delivery of mTHPC nanoparticulate formation to colorectal cancer cells for photodynamic therapy are limited. Millard *et al* (2020) used ~203 nm mTHPC-loaded extracellular vesicles (EV) and compared them with Foslip in a colorectal HT29 murine xenograft mouse model (42). They showed that in 3D cancer cell models, mTHPC-EV uptake produced deeper penetration after 24 h incubation as compared to Foslip, whilst *in vivo* results showed a 33% increase in tumour killing with PDT treatment applied 24 h after injection but 0% was observed after Foslip-mediated PDT. However, a concerning finding was the big difference between liposomal and EV formulations in mTHPC-EV accumulation in the lung (five to seven times higher than Foslip) and liver. In sharp contrast, our data showed that significant fluorescence was only observed in the hepatobiliary system, which peaked at 24 h and reduced by 48 h post-injection. Other studies that investigated the biodistribution and excretion of silica nanoparticles have reported similar findings (43-45). Bretin *et al.* (2019) demonstrated the usefulness of nanoparticle encapsulation for PDT tumour targeting efficacy in CRC (46). They used 80 nm silica nanoparticles coated with xylan to encapsulate 5-(4-hydroxyphenyl)-10,15,20-triphenylporphyrin (TPPOH) and tested it in a colorectal HT-29 murine

View Article Online
DOI: 10.1039/D3NR04118B

xenograft mouse model. They showed significant phototoxic effects of TPPOH-X SNPs mediated by ROS generation and stronger cell uptake in human colorectal cancer compared to free TPPOH. Abdelghany *et al* (2013) successfully encapsulated meso-tetra(N-methyl-4-pyridyl) porphine tetra tosylate (TMP) photosensitiser in a hydrogel-based chitosan/ alginate nanosystem with an anti-death-receptor-5 (DR5) antibody tagged onto the surface (47). Although their nanoparticle elicited a more potent phototoxic effect than free drug, the nanoparticle diameter was prohibitively large at 560 nm. In addition, DR5 is not specific to colorectal cancer and is not highly expressed. Others have reported successful encapsulation of mTHPC in nanoparticles for photodynamic therapy in colorectal cancer cells, but without a surface targeting molecule (48). To date, Foslip has been intensively tested in different *in vitro* preclinical models (2D and 3D tumour cell cultures) (34, 49, 50), whilst PDT studies, including biodistribution, pharmacokinetics, and PDT efficacy in tumour-bearing *in vivo* animal models are limited (51, 52).

The surgical management of colorectal cancer is often limited by difficulty in delineating tumour margins and an inability to visualise occult nodal metastasis. This predisposes to tumour recurrence and decreased survival. Although several studies have investigated the efficacy of PSs for PDT regimens in CRC, only few have meticulously explored their application for fluorescence imaging. We have shown that CEA-Fos-NPs enabled real-time fluorescence imaging of colorectal tumours, accurately distinguishing tumour from normal tissue. Gavrina *et al.* (2018), investigated Chlorin e6 (Ce6) conjugated to polyvinyl alcohol (PVA) nanoparticles for *in vivo* fluorescence imaging in CT26 xenograft model (53). The authors found a higher tumour-to-normal signal in mice treated with Ce6–PVA nanoparticles when compared to Ce6 alone. Xu *et al* (2018) fabricated a H_2S-responsive NIR-fluorescent silica based

NPs which allowed fluorescent imaging in HCT116 CRC cells, both *in vitro* and *in vivo* (54). The study design lacked control NPs and control cell lines while for the *in vivo* experiment the NPs were injected into the core of the tumour xenograft and not systemically. Soster *et al* (2012), used PEG-conjugated dye-doped silica nanoparticles, via systemic delivery, to image CRC metastases in murine xenograft models (55). They used 'bare' nanoparticles as controls and imaged fluorescence only in *ex vivo* organs, raising concerns for antigen-specific targeting.

View Article Online
DOI: 10.1039/D3NR04118B

Conclusion

We have successfully developed a unique targeting strategy to deliver Foslip to colorectal cancer in an animal model using a novel Affimer protein. We have shown that Affimer tagged silica coated Foslip nanoparticles are effective theranostic agents. The nanoparticle design enables stable assembly of the components within a small sized structure, with favourable pharmacokinetic profile and biodistribution, and superior cellular uptake. Our nanoparticle is potentially applicable to targeting other solid tumours by changing the surface Affimer and provided that there is a specific tissue biomarker.

View Article Online
DOI: 10.1039/D3NR04118B

Materials and Methods

Synthesis of silica coated Foslip nanoparticles

All experiments were performed at room temperature using Sigma-Aldrich (USA) reagents unless otherwise stated. Nanoparticles synthesis was modified from previous publications (22, 26).

Water soluble meta-tetra (hydroxyphenyl) chlorin (mTHPC) Foslip® photosensitiser (20 mg/mL DPPC/DPPG, 2.2 mM mTHPC, 50 mg/mL glucose) was provided by Biolitec AG (Jena, Germany) with molecular weight of 680.764 g/mol. The powder was dissolved in PBS to make a stock solution of 100 µM and filtered through a syringe filter (0.1 µm pore size; TPP, Trasadingen, Switzerland). Tetraethyl orthosilicate (TEOS) was added (12 µL) into 1 mL of deionised water and stirred at 200 rpm for 24 h at room temperature. Next, 20 µL of the Foslip suspension was added to the TEOS solution and the mixture was stirred at 200 rpm for 1 h. Two mL of PBS (1x) buffer solution was added to the mixture and stirred for 30 min then 24 µL of fresh TEOS were added and the mixture was stirred at 200 rpm for 48 h. The mixture was then transferred into Corex centrifuge tubes (Corning) with equal volumes. Particles were pelleted by centrifugation (15,000 ×g, 25 min), resuspended in wash solution using ultrasound sonication, repelleted and the supernatant discarded. This wash step was repeated three times before the liquid was discarded and the particles were resuspended in 0.1 M PBS at a concentration of 1 mg/mL using sonication then stored at 4 °C.

APTES amination

Freshly synthesised nanoparticles were suspended in 1 mL of ethanol plus 4% [v/v] (3-aminopropyl) triethoxysilane (APTES) and stirred at 200 rpm for 3 h at room temperature while stirring in a Falcon tube. The aminated particles were then

View Article Online
DOI: 10.1039/D3NR04118B

transferred to a centrifuge tube (Corex) followed by 2x washes with ethanol and centrifuged at 11,000 xg for 25 min. The contents were then washed once using 2-(*N*-morpholino) ethanesulfonic acid (MES) buffer (pH 7.0) then resuspended in MES buffer at final concentration of 1 mg/mL.

Affimer production

Anti CEA specific Affimer clones were identified using a 'phage display library' method as recently published by Shamsuddin *et al* (30, 31). Out of the three CEA binding Affimers identified, clone II and III (molecular weight 12.5 and 12.6 kDa respectively) were chosen for this study having 9 and 10 distinct amino acid residues at the variable region respectively. Anti-human cardiac myoglobin Affimer was used as a control. Anti-CEA (II and III) and control Affimer clone (molecular weight 12.5 kDa) DNA were isolated as previously described and the Affimer protein were expressed from a pET11a vector in BL21 (DE3) *E.coli* cells. The *E.coli* cells were grown in Luria-Bertani broth medium containing 100 µg/mL of carbinicillin until the growth was 0.8 at A_{600}. Then cells were induced with 0.1 mM IPTG and incubated at 25 °C for 6 hours. The cells were harvested by centrifugation, lysed and the His_6 tagged Affimers were purified on Ni^{2+}-NTA affinity chromatography (Merck, New Jersey, USA). Pierce® Immobilised tris (2-carboxyethyl) phosphine (TCEP) reducing gel was used to reduce Affimer disulphide bonds to free all thiol groups for subsequent maleimide coupling chemistry. TCEP gel (150 µL) was washed with PBS containing 1 mM edetate disodium (EDTA) three times followed by 4 µL of PBS containing 50 mM EDTA, followed by adding of 150 µL of 0.5 mg/mL Affimer. The mixture was stirred at 20 rpm for 1 h then centrifuged at 1,000 xg for 1 min and finally reduced Affimers were recovered from the supernatant.

View Article Online
DOI: 10.1039/D3NR04118B

Silica nanoparticle Affimer conjugation

Fresh sulfo-succinimidyl 4-(maleimidomethyl) cyclohexane-1-carboxylate (SMCC) (6 mg) was mixed with 60 µg (1 mg/mL) of polyclonal anti-CEA or anti-myoglobin Affimers and stirred gently at room temperature for 20 minutes. The reaction mixture was then added to 4 mL of 1 mg/mL aminated nanoparticles and stirred at room temperature for 2 h then washed twice with PBS (6,000 xg for 15 min) to remove unbound sulfo-SMCC. The nanoparticles were resuspended at 2 mg/mL and finally 0.1% (w/v) BSA was added. The nanoparticles were either stored in the dark at 4 °C or used immediately for *in vitro* experiments.

Scanning electron microscopy (SEM)

SEM images were obtained with a field emission gun scanning electron microscopy (FEG-SEM, LEO 1530 Gemini FEGSEM) fitted with an Oxford Instruments 80 mm X-Max SDD detector, Carl Zeiss.

Spectrofluorometer measurements of silica nanoparticles

The fluorescence intensity of silica coated nanoparticles was quantified on a spectrofluorometer (Berthold Technologies Mithras LB 940 multimode microplate reader with Mikro Win 2000 software) with a halogen lamp intensity of 23,000 and excitation and emission spectra of 645 nm +/- 30 nm.

Affimer per nanoparticle quantification assay

Affimer tagged NPs were suspended in PBS at 1 mg/mL then mixed with 5 mL of 2-mercaptoethanol 1% (v/v) and incubated for 1 h at 37 °C. The suspension was then centrifuged at at 12,500 xg for 30 min. The supernatant was recovered; then desalted using a Zepa spin desalting column (7K MWCO) to remove any remnants that might interfere with the fluorescent dye NanoOrange®. The released Affimers were quantified using a NanoOrange® protein quantitation kit.

View Article Online
DOI: 10.1039/D3NR04118B

Standard solutions of Affimer (0 – 2.5 µg) were prepared in 1X NanoOrange® reagent working solution from 10 µg/mL stock solutions. For sample analysis, 10 µl of each desalted solution was mixed with 240 µl of 1X NanoOrange® working solution. All standard and sample solutions were prepared in 500 µL tubes and incubated at 95 ºC in a water bath for 10 min. All processes were carried out protected from light. The samples were allowed to cool down at RT for 20 min before 200 µL of each solution was transferred to a 96-well plate for fluorescence intensity measurement. The measurement was carried out with excitation and emission wavelengths of 485 nm and 590 nm, respectively. The fluorescence values of the standards and samples were subtracted from the value of reagent blank. The corrected values were used in generating calibration curves using Graphprism and linear fitting was performed.

Dynamic light scattering (DLS)

The DLS measurement for nanoparticles was made using a Zetasizer Nano series, Nano-ZS DLS system with a red (633 nm) laser (Malvern Instruments Ltd) at room temperature and in a small volume disposable cuvette. The polydispersity index (PDI) of the colloidal solutions was measured using DLS with a particle size analyser. The zeta potential or overall surface charge of each nanoparticle sample in solution (~1 mg/mL in millipore water) was determined using a Zeta Plus, zeta potential analyser (Brookhaven Instruments Corp. Holtsville, NY).

Nanoparticle-mediated fluorescent imaging *in vitro*

HEK293 epithelial cell line, as a control, and the human colorectal cancer cell lines, LoVo, HCT116, and LS174T, were obtained from the American Type Culture Collection (ATCC). HEK293 cells were maintained in DMEM (1X) with GlutaMAX™-I (Gibco®) and 10% (v/v) FBS (Sigma life Science). Cancer cells were maintained in Advanced MEM (ATCC) for LoVo, F12K Nutrimix (Invitrogen, USA) for LS174T and

View Article Online
DOI: 10.1039/D3NR04118B

RPMI 1640 (Invitrogen, USA) for HCT116. All cells were supplemented with 10% FCS and 1% L-glutamine at 37 °C in 5% CO_2. Cells ($9x10^4$) were seeded onto sterile glass coverslips (Cellpath, Newtown Powys, UK) in a six-well plate (Corning) and incubated at 37 °C in 5% CO_2 for 24 h. Culture media was discarded and cells were washed 2x with PBS followed by addition of paraformaldehyde (4%, v/v) for fixation. Following incubation for 30 min at room temperature, the fixative was removed and cells were washed 3x times with PBS. BSA (0.1% (w/v), (EMD chemicals, San Diego, USA)) was added for 30 min then followed by 3x washes with PBS. Anti-CEA or anti-myoglobin Affimer tagged nanoparticles (1 mg/mL) were added to the wells and incubated for 24 h in the dark at room temperature. The nanoparticle suspension was discarded and the cells were washed 3x times with PBS then coverslips were mounted onto glass slides using Depex (Waltham, Massachusettes, USA). The slides were left to cure overnight then stored at 4 °C in the dark and imaged using confocal microscopy. Images were captured using a Nikon A1R-A1 confocal microscope (Nikon, Japan) with NHS Elements software (v 4.0). ImageJ v1.42q (NIH Freeware, USA) was used to quantify fluorescence.

Nanoparticles internalisation and co-localisation *in vitro*

LoVo and LS174T cells ($2x10^4$) were seeded onto sterile coverslips and allowed to adhere overnight. The following day, cells were treated with fluorescein isothiocyanate (FITC) and CEA- or Myo-Affimer tagged-nanoparticles (1 mg/mL) for 1, 4 and 24 hours. Cells were washed three times with PBS to remove nanoparticle suspension and incubated with LysoTracker™ deep red (Thermofisher) at 50 nM for 1 h. Following three washes with PBS, cells were fixed with 4% PFA. Following routine wash, nucleus was counterstained with DAPI and mounted onto slides using mounting media

View Article Online
DOI: 10.1039/D3NR04118B

(Fluoroshield, Sigma). To monitor NPs uptake, imaging was performed at 100x magnification using a fluorescent microscope.

Photodynamic therapy and cell cytotoxicity *in vitro*

LoVo, LS174T, HCT116 and HEK293 cells were grown in two identical 6 well plates. Anti-CEA Affimer tagged nanoparticles and their respective controls with various concentrations (1-5 mg/mL) were added to the wells and incubated for 24 h in the dark at room temperature. The nanoparticle suspension was removed after 24 h and the cells were washed 3x times with PBS the incubated with fresh media. The plates were then immediately placed on top of a light-radiating device (Avago Technologies, California, USA). Cells were treated with a light dose of 0.225 - 0.675 J/cm^2, peak wavelength of 600-700 nm and a spectral half-width of 12 nm, then kept in the dark. Light dose was calculated based on treatments which lasted for 10-45 min at 0.25 mW/cm^2. Control plates were kept in the dark with no light irradiation.

Stock solution of 3-[4,5-dimethylthiazole-2-yl]-2,5-diphenyltetrazolium bromide (MTT) tetrazolium salt MTT (Sigma) was prepared at 5 mg/mL in PBS and wrapped in foil to protect from light. The media, in which the seeded cells were grown, was replaced with 50 µL of 1 mg/mL working MTT solution and incubated in the dark for 3 hours. MTT solution was then removed and the dark blue formazan dye formed was dissolved in 100 µL of propan-1-ol. Optical density was measured using a microplate reader (Opsys MR^{TM}, Dynex technologies ltd, UK) at 570 nm.

Cellular reactive oxygen species detection assay

Cells were seeded on a 96 well plate 2.5 x 10^4 cells/well and incubated for 24 h. Cells were then washed once using 1X Buffer then stained with 25 µM 2',7' – dichlorofluorescin diacetate (DCFDA) in 1X Buffer for 45 min at 37 °C. Cells were then washed once with PBS then incubated with functionalised silica nanoparticles for 24

View Article Online
DOI: 10.1039/D3NR04118B

h in the dark then illuminated for 30 min. Immediately after illumination, nanoparticles suspension was then discarded and 10 μM DCF-DA (Merck, New Jersey, USA) in Hank's balance salt solution (Merck, New Jersey, USA) was added for 30 min and incubated in a CO_2 incubator then washed with PBS. DCF fluorescence was observed using confocal microscope.

Fluorescent imaging *in vivo*

The *in vivo* experiments were conducted in a UK Home Office designated animal facility at Leeds Institute of Medical Research (University of Leeds, UK). The study was conducted in line with UK Home Office regulations and in accordance with The Animals (Scientific Procedures) Act 1986, under a personal animal licence (Licence number: P93AOF172). BALB/c nu/nu female mice (4-6 weeks old) (Charles River, UK) were injected subcutaneously with 1.5×10^6 LS174T cells to the right flank. Tumour xenografts were developed to nearly 10 mm in diameter within ~ 10 days, then mice were randomised to either CEA-targeted or control Affimer tagged-nanoparticles. Mice were injected with nanoparticles at 150 μL (suspended in sterile PBS at 2 mg/mL concentration) via the tail vein under general anaesthesia. Fluorescent images were captured using IVIS imaging (filters: excitation 672 nm, emission 694 nm; Perkin Elmer, USA) under anaesthesia then imaged at different time points. Living Image (v4.3.1, Caliper Life Sciences, USA); was used for fluorescence measurements (radiant efficiency in (p/s/cm^2/sr) / (μW/cm^2)) after calibration to background. *Ex vivo* fluorescence imaging was performed on all the resected tumour xenografts and the remaining organs.

Photodynamic Therapy *in vivo*

The PDT efficacy of Foslip encapsulated silica nanoparticles was evaluated in LS174T CRC xenograft models *in vivo*. Animal models were categorised into four treatment

groups: i) anti-CEA Affimer targeted NPs plus PDT laser treatment, ii) anti-myoglobin targeted NPs plus PDT laser treatment, iii) anti-CEA targeted NPs alone and iv) anti-myoglobin targeted NPs alone. Tumour xenograft volumes, mice weights and Body Conditioning Scoring were recorded before and after PDT experiment. Mice were anaesthetised then immobilised in plexi-glass holders 24 h post intravenous injection then irradiated at the xenografts using 650 nm fibre optic laser. The laser was positioned 18 mm directly above the skin, delivering a total light dose of 50 J/cm^2, at a fluence rate of 60 mW/cm^2 resulting in a total irradiation time of 14 min. Thermal imaging videos were recorded for 1 min at 0, 7 and 14 min during treatment for each mouse. Mice were maintained and monitored for 5 days post PDT treatment. Following completion of the experiment, mice were euthanised in accordance with Schedule 1 of the Animals (Scientific Procedures) Act 1986 and the tumour xenografts and organs were harvested. The efficacy of PDT was evaluated by histological analysis in harvested tissue.

Statistical analysis

GraphPad Prism Version 9.0 (GraphPad Software, California, USA) was used for the statistical analysis of all the data. The difference between the groups were evaluated using Student's t-test and Wilcoxon Signed Rank Test.

Financial & competing interests disclosure

This work was supported by a MRC fellowship and AMS grant awarded to YSK. The authors have no other relevant affiliations or financial involvement with any organisation or entity with a financial interest in or financial conflict with the subject matter or materials discussed in the manuscript apart from those disclosed.

No writing assistance was utilised in the production of this manuscript.

View Article Online
DOI: 10.1039/D3NR04118B

Author Contributions

Y.S.K, P.A.M, T.A.H and D.G.J conceived and designed the experiments. E.A and S.H.S performed the Affimer expression and purification. M.I.K, T.M, N.L, A.P and Y.S.K performed the *in vivo* experiments and analysed the data. R.A-M performed fluorescent microscopy experiments. Y.S.K performed all the other experiments and analysed the data. L.C. contributed to design of the *in vivo* experiments. A.P, D.T, L.C, D.G.J, T.A.H, P.A.M and J.T contributed to study design. All authors interpreted the results. Y.S.K, P.A.M, T.A.H and D.G.J co-wrote the manuscript. All authors discussed the results and commented on the manuscript.

Acknowledgments

The authors would like to thank the MRC, UK and AMS, UK for the doctoral fellowship and starter grant awarded to Y.S.K. We thank Dr. Nicola Ingram from the Leeds Institute of Medical Research at the University of Leeds for her support with the animal studies. We thank Prof. M.J McPherson, Director of BHRC BioScreening Technology Group, and Prof P. Jones, Director of the Leeds Institute of Medical Research at St James's Hospital for their support and assistance.

View Article Online
DOI: 10.1039/D3NR04118B

References

1. Hansdotter P, Scherman P, Petersen S, Mikalonis M, Holmberg E, Rizell M, et al. Patterns and resectability of colorectal cancer recurrences: outcome study within the COLOFOL trial. BJS open. 2021;5(4):zrab067.
2. Malakorn S, Ouchi A, Hu C-Y, Sandhu L, Dasari A, You Y-QN, et al. Tumor sidedness, recurrence, and survival after curative resection of localized colon cancer. Clinical colorectal cancer. 2021;20(1):e53-e60.
3. Osterman E, Glimelius B. Recurrence risk after up-to-date colon cancer staging, surgery, and pathology: analysis of the entire Swedish population. Diseases of the Colon & Rectum. 2018;61(9):1016-25.
4. Rahbari NN, Bork U, Motschall E, Thorlund K, Buchler MW, Koch M, et al. Molecular detection of tumor cells in regional lymph nodes is associated with disease recurrence and poor survival in node-negative colorectal cancer: a systematic review and meta-analysis. Journal of clinical oncology : official journal of the American Society of Clinical Oncology. 2012;30(1):60-70.
5. Elferink M, Visser O, Wiggers T, Otter R, Tollenaar R, Langendijk J, et al. Prognostic factors for locoregional recurrences in colon cancer. Annals of surgical oncology. 2012;19(7):2203-11.
6. Sinicrope FA. Increasing Incidence of Early-Onset Colorectal Cancer. New England Journal of Medicine. 2022;386(16):1547-58.
7. Xi Y, Xu P. Global colorectal cancer burden in 2020 and projections to 2040. Translational Oncology. 2021;14(10):101174.
8. Hapuarachchige S, Artemov D. Theranostic pretargeting drug delivery and imaging platforms in cancer precision medicine. Frontiers in oncology. 2020;10:1131.
9. Siddique S, Chow JC. Recent Advances in Functionalized Nanoparticles in Cancer Theranostics. Nanomaterials. 2022;12(16):2826.
10. Tada DB, Baptista MS. Photosensitizing nanoparticles and the modulation of ROS generation. Frontiers in chemistry. 2015;3:33.
11. Yu Z, Pan W, Li N, Tang B. A nuclear targeted dual-photosensitizer for drug-resistant cancer therapy with NIR activated multiple ROS. Chemical science. 2016;7(7):4237-44.
12. Kaleta-Richter M, Kawczyk-Krupka A, Aebisher D, Bartusik-Aebisher D, Czuba Z, Cieslar G. The capability and potential of new forms of personalized colon cancer treatment: Immunotherapy and Photodynamic Therapy. Photodiagnosis Photodyn Ther. 2019;25:253-8.
13. Senge MO, Brandt JC. Temoporfin (Foscan(R), 5,10,15,20-tetra(m-hydroxyphenyl)chlorin)--a second-generation photosensitizer. Photochemistry and photobiology. 2011;87(6):1240-96.
14. Millard M, Yakavets I, Piffoux M, Brun A, Gazeau F, Guigner JM, et al. mTHPC-loaded extracellular vesicles outperform liposomal and free mTHPC formulations by an increased stability, drug delivery efficiency and cytotoxic effect in tridimensional model of tumors. Drug Deliv. 2018;25(1):1790-801.
15. Maeda H, Tsukigawa K, Fang J. A Retrospective 30 Years After Discovery of the Enhanced Permeability and Retention Effect of Solid Tumors: Next-Generation Chemotherapeutics and Photodynamic Therapy--Problems, Solutions, and Prospects. Microcirculation. 2016;23(3):173-82.
16. Fahmy SA, Azzazy HME-S, Schaefer J. Liposome photosensitizer formulations for effective cancer photodynamic therapy. Pharmaceutics. 2021;13(9):1345.
17. Reshetov V, Zorin V, Siupa A, D'Hallewin MA, Guillemin F, Bezdetnaya L. Interaction of liposomal formulations of meta-tetra (hydroxyphenyl) chlorin (temoporfin) with serum proteins: protein binding and liposome destruction. Photochemistry and photobiology. 2012;88(5):1256-64.
18. Millard M, Yakavets I, Piffoux M, Brun A, Gazeau F, Guigner J-M, et al. mTHPC-loaded extracellular vesicles outperform liposomal and free mTHPC formulations by an

View Article Online
DOI: 10.1039/D3NR04118B

910 increased stability, drug delivery efficiency and cytotoxic effect in tridimensional model of
911 tumors. Drug delivery. 2018;25(1):1790-801.
912 19. van der Meel R, Fens MH, Vader P, Van Solinge WW, Eniola-Adefeso O, Schiffelers
913 RM. Extracellular vesicles as drug delivery systems: lessons from the liposome field. Journal
914 of controlled release. 2014;195:72-85.
915 20. Hadinoto K, Sundaresan A, Cheow WS. Lipid-polymer hybrid nanoparticles as a new
916 generation therapeutic delivery platform: a review. Eur J Pharm Biopharm. 2013;85(3 Pt
917 A):427-43.
918 21. Ingle SG, Pai RV, Monpara JD, Vavia PR. Liposils: An effective strategy for
919 stabilizing Paclitaxel loaded liposomes by surface coating with silica. European Journal of
920 Pharmaceutical Sciences. 2018;122:51-63.
921 22. Begarani F, Cassano D, Margheritis E, Marotta R, Cardarelli F, Voliani V. Silica-
922 based nanoparticles for protein encapsulation and delivery. Nanomaterials. 2018;8(11):886.
923 23. Chen S, Greasley S, Ong Z, Naruphontjirakul P, Page S, Hanna J, et al.
924 Biodegradable zinc-containing mesoporous silica nanoparticles for cancer therapy. Materials
925 Today Advances. 2020;6:100066.
926 24. Anselmo AC, Mitragotri S. Nanoparticles in the clinic: An update. Bioengineering &
927 translational medicine. 2019;4(3):e10143.
928 25. Tiernan J, Perry S, Verghese E, West N, Yeluri S, Jayne D, et al. Carcinoembryonic
929 antigen is the preferred biomarker for in vivo colorectal cancer targeting. British journal of
930 cancer. 2013;108(3):662.
931 26. Tiernan JP, Ingram N, Marston G, Perry SL, Rushworth JV, Coletta PL, et al. CEA-
932 targeted nanoparticles allow specific in vivo fluorescent imaging of colorectal cancer models.
933 Nanomedicine. 2015;10(8):1223-31.
934 27. Baker M. Reproducibility crisis: Blame it on the antibodies. Nature News.
935 2015;521(7552):274.
936 28. Bradbury AR, Plückthun A. Getting to reproducible antibodies: the rationale for
937 sequenced recombinant characterized reagents. Protein Engineering, Design and Selection.
938 2015;28(10):303-5.
939 29. Tiede C, Bedford R, Heseltine SJ, Smith G, Wijetunga I, Ross R, et al. Affimer
940 proteins are versatile and renewable affinity reagents. Elife. 2017;6.
941 30. Shamsuddin SH, Jayne DG, Tomlinson DC, McPherson MJ, Millner PA. Selection
942 and characterisation of Affimers specific for CEA recognition. Sci Rep. 2021;11(1):744.
943 31. Shamsuddin SH, Gibson TD, Tomlinson DC, McPherson MJ, Jayne DG, Millner PA.
944 Reagentless Affimer- and antibody-based impedimetric biosensors for CEA-detection using
945 a novel non-conducting polymer. Biosens Bioelectron. 2021;178:113013.
946 32. Li C, Zhang Y, Su T, Feng L, Long Y, Chen Z. Silica-coated flexible liposomes as a
947 nanohybrid delivery system for enhanced oral bioavailability of curcumin. Int J
948 Nanomedicine. 2012;7:5995-6002.
949 33. Begu S, Aubert Pouessel A, Lerner DA, Tourne-Peteilh C, Devoisselle JM. Liposil, a
950 promising composite material for drug storage and release. J Control Release.
951 2007;118(1):1-6.
952 34. Yakavets I, Millard M, Lamy L, Francois A, Scheglmann D, Wiehe A, et al.
953 Matryoshka-type liposomes offer the improved delivery of temoporfin to tumor spheroids.
954 Cancers. 2019;11(9):1366.
955 35. Pereira I, Sousa F, Kennedy P, Sarmento B. Carcinoembryonic antigen-targeted
956 nanoparticles potentiate the delivery of anticancer drugs to colorectal cancer cells. Int J
957 Pharm. 2018;549(1-2):397-403.
958 36. Yang X, Zhuo Y, Zhu S, Luo Y, Feng Y, Xu Y. Selectively assaying CEA based on a
959 creative strategy of gold nanoparticles enhancing silver nanoclusters' fluorescence. Biosens
960 Bioelectron. 2015;64:345-51.
961 37. Ma L, Chen Q, Ma P, Han MK, Xu Z, Kang Y, et al. iRGD-functionalized PEGylated
962 nanoparticles for enhanced colon tumor accumulation and targeted drug delivery.
963 Nanomedicine (Lond). 2017;12(16):1991-2006.

964 38. Li J, Zhou C, Dong B, Zhong H, Chen S, Li Q, et al. Single domain antibody-based
965 bispecific antibody induces potent specific anti-tumor activity. Cancer Biol Ther.
966 2016;17(12):1231-9.
967 39. Fan X, Wang T, Han M, Gu Y, Sun G, Peng X, et al. Dual CEA/CD44 targeting to
968 colorectal cancer cells using nanobody-conjugated hyaluronic acid-modified mesoporous
969 silica nanoparticles with pH-and redox-sensitivity. Materials Advances. 2022.
970 40. Cheng WW, Allen TM. The use of single chain Fv as targeting agents for
971 immunoliposomes: an update on immunoliposomal drugs for cancer treatment. Expert Opin
972 Drug Deliv. 2010;7(4):461-78.
973 41. Pramanik A, Xu Z, Shamsuddin SH, Khaled YS, Ingram N, Maisey T, et al. Affimer
974 Tagged Cubosomes: Targeting of Carcinoembryonic Antigen Expressing Colorectal Cancer
975 Cells Using In Vitro and In Vivo Models. ACS Appl Mater Interfaces. 2022;14(9):11078-91.
976 42. Millard M, Posty S, Piffoux M, Jasniewski J, Lassalle HP, Yakavets I, et al. mTHPC-
977 Loaded Extracellular Vesicles Significantly Improve mTHPC Diffusion and Photodynamic
978 Activity in Preclinical Models. Pharmaceutics. 2020;12(7).
979 43. Park J-H, Gu L, Von Maltzahn G, Ruoslahti E, Bhatia SN, Sailor MJ. Biodegradable
980 luminescent porous silicon nanoparticles for in vivo applications. Nature materials.
981 2009;8(4):331-6.
982 44. Souris JS, Lee C-H, Cheng S-H, Chen C-T, Yang C-S, Ho J-aA, et al. Surface
983 charge-mediated rapid hepatobiliary excretion of mesoporous silica nanoparticles.
984 Biomaterials. 2010;31(21):5564-74.
985 45. Sarparanta M, Bimbo LM, Rytkönen J, Mäkilä E, Laaksonen TJ, Laaksonen Pi, et al.
986 Intravenous delivery of hydrophobin-functionalized porous silicon nanoparticles: stability,
987 plasma protein adsorption and biodistribution. Molecular pharmaceutics. 2012;9(3):654-63.
988 46. Bretin L, Pinon A, Bouramtane S, Ouk C, Richard L, Perrin ML, et al. Photodynamic
989 Therapy Activity of New Porphyrin-Xylan-Coated Silica Nanoparticles in Human Colorectal
990 Cancer. Cancers (Basel). 2019;11(10).
991 47. Abdelghany SM, Schmid D, Deacon J, Jaworski J, Fay F, McLaughlin KM, et al.
992 Enhanced antitumor activity of the photosensitizer meso-tetra (N-methyl-4-pyridyl) porphine
993 tetra tosylate through encapsulation in antibody-targeted chitosan/alginate nanoparticles.
994 Biomacromolecules. 2013;14(2):302-10.
995 48. Löw K, Knobloch T, Wagner S, Wiehe A, Engel A, Langer K, et al. Comparison of
996 intracellular accumulation and cytotoxicity of free mTHPC and mTHPC-loaded PLGA
997 nanoparticles in human colon carcinoma cells. Nanotechnology. 2011;22(24):245102.
998 49. Gibot L, Lemelle A, Till U, Moukarzel Ba, Mingotaud A-Fo, Pimienta Vr, et al.
999 Polymeric micelles encapsulating photosensitizer: structure/photodynamic therapy efficiency
1000 relation. Biomacromolecules. 2014;15(4):1443-55.
1001 50. Gaio E, Scheglmann D, Reddi E, Moret F. Uptake and photo-toxicity of Foscan®,
1002 Foslip® and Fospeg® in multicellular tumor spheroids. Journal of Photochemistry and
1003 Photobiology B: Biology. 2016;161:244-52.
1004 51. Lassalle H-P, Dumas D, Gräfe S, D'Hallewin M-A, Guillemin F, Bezdetnaya L.
1005 Correlation between in vivo pharmacokinetics, intratumoral distribution and photodynamic
1006 efficiency of liposomal mTHPC. Journal of controlled release. 2009;134(2):118-24.
1007 52. Brezániová I, Záruba K, Králová J, Adámková H, Ulbrich P, Poučková P, et al. Silica-
1008 based nanoparticles are efficient delivery systems for temoporfin. Photodiagnosis and
1009 photodynamic therapy. 2018;21:275-84.
1010 53. Gavrina AI, Shirmanova MV, Aksenova NA, Yuzhakova DV, Snopova LB, Solovieva
1011 AB, et al. Photodynamic therapy of mouse tumor model using chlorin e6- polyvinyl alcohol
1012 complex. Journal of photochemistry and photobiology B, Biology. 2018;178:614-22.
1013 54. Xu G, Yan Q, Lv X, Zhu Y, Xin K, Shi B, et al. Imaging of Colorectal Cancers Using
1014 Activatable Nanoprobes with Second Near-Infrared Window Emission. Angew Chem Int Ed
1015 Engl. 2018;57(14):3626-30.
1016 55. Soster M, Juris R, Bonacchi S, Genovese D, Montalti M, Rampazzo E, et al.
1017 Targeted dual-color silica nanoparticles provide univocal identification of micrometastases in

1018 preclinical models of colorectal cancer. International Journal of Nanomedicine. 2012;7:4797-
1019 807.
1020